IEICE TRANS. ELECTRON., VOL.E83–C, NO.3 MARCH 2000

PAPER

LAPAREX–An Automatic Parameter Extraction Program for Gain- and Index-Coupled Distributed Feedback Semiconductor Lasers, and Its Application to Observation of Changing Coupling Coefficients with Currents

Toru NAKURA[†], ***Nonmember and*** **Yoshiaki NAKANO**[†a)], ***Member***

SUMMARY A reliable and automatic parameter extraction technique for DFB lasers is developed. The parameter extraction program which is named "LAPAREX" is able to determine many device parameters from a measured sub-threshold spectrum only, including gain- and index-coupling coefficients, and spatial phases of the grating at front and rear facets. Injection current dependence of coupling coefficients in a gain-coupled DFBlaser is observed, for the first time, by making use of it.

key words: *distributed feedback semiconductor lasers, DFB lasers, parameter extraction, coupling coefficient, gain coupling*

1. Introduction

Determination of device parameters in distributed feedback (DFB) lasers is very important for optimization of laser characteristics as well as for system design. Among several device parameters, the coupling coefficient is the most important but its determination has only been possible in anti-reflection (AR) coated index-coupled DFB lasers. Moreover, this is not an easy task or not very accurate if there are facet reflectivities remaining [1], [2]. There has been no way to measure the gain-coupling coefficient in gain-coupled DFB lasers, which is the largest issue that needs to be solved before they are practically utilized.

Besides the coupling coefficient evaluation, the spatial phase of the grating should be determined since it affects laser performance significantly when facet reflectivity exists. Nevertheless, there have only been few and complicated ways to measure it [3].

The purpose of this paper is to provide an easy and nondestructive parameter extraction method that is applicable to both index- and gain-coupled DFB lasers with facet reflection. The method we present here uses numerical fitting of theoretical sub-threshold spectrum into measured one by the least-square algorithm [4]. The program developed here is named "LAPAREX" which is an abbreviation of "Laser PARameter EXtraction." In Sect. 2, the model of theoretical sub-threshold spectrum is shown. In Sect. 3, the details of numerical fitting, such as how to determine initial parameters, are explained. In Sect. 4, error estimation method of extracted parameters are given. Section 5 describes observation of changing coupling coefficients in a gain-coupled DFB laser with absorptive grating for the first time [5]. Summary and conclusions are given in the final section.

Manuscript received September 21, 1999.
Manuscript revised November 22, 1999.

[†]The authors are with the Dept. of Electronic Engineering, the Univ. of Tokyo, Tokyo, 113-8656 Japan.
a) E-mail: nakano@ee.t.u-tokyo.ac.jp

2. Model

2.1 Spectrum Calculation

The model of theoretical sub-threshold spectrum is based on the static coupled-mode equations [6]:

$$\frac{\partial R^+}{\partial z} - (\alpha - j\delta)R^+ = -j\kappa e^{-j\theta_l} R^- \tag{1}$$

$$-\frac{\partial R^-}{\partial z} - (\alpha - j\delta)R^- = -j\kappa e^{j\theta_l} R^+ \tag{2}$$

$$E^+(z) = R^+(z)e^{-j\beta_0 z} \tag{3}$$

$$E^-(z) = R^-(z)e^{j\beta_0 z} \tag{4}$$

where z is the axial coordinate, R^+ and R^- the amplitudes of the forward and backward propagating fields, E^+ and E^-, β_0 the propagation constant at Bragg wavelength, 2α ($\equiv \Gamma g - \alpha_i$) the net gain, δ the deviation of the propagation constant from β_0, θ_l the spatial phase of the grating at rear facet ($z = 0$), and κ the coupling coefficient, respectively.

Equations (1) and (2) are manipulated by the transfer matrix method [7], [8], where R^+ and R^- at $z = z + l$ can be calculated by

$$\begin{pmatrix} R^+(z+l) \\ R^-(z+l) \end{pmatrix} = \begin{pmatrix} F_{11}(l) & F_{12}(l) \\ F_{21}(l) & F_{22}(l) \end{pmatrix} \begin{pmatrix} R^+(z) \\ R^-(z) \end{pmatrix} \tag{5}$$

in which

$$F_{11}(l) \equiv \cosh(Dl) - j\frac{\Delta\beta}{D}\sinh(Dl) \quad (6)$$

$$F_{12}(l) \equiv -j\frac{\kappa^+}{D}\sinh(Dl) \quad (7)$$

$$F_{21}(l) \equiv j\frac{\kappa^-}{D}\sinh(Dl) \quad (8)$$

$$F_{22}(l) \equiv \cosh(Dl) + j\frac{\Delta\beta}{D}\sinh(Dl) \quad (9)$$

and

$$\Delta\beta \equiv \left\{\frac{2\pi}{\lambda}n + j\frac{1}{2}(\Gamma g - \alpha_i)\right\} - \beta_0 = \delta - j\alpha \quad (10)$$

$$D^2 \equiv -(\Delta\beta)^2 + \kappa^2. \quad (11)$$

Here, λ is the wavelength, n the effective index of refraction, g the active layer bulk gain, Γ the optical confinement factor into the active layer, and α_i the propagation loss.

Because R^+ and R^- are related to E^+ and E^- by Eqs. (3) and (4), the relations among $E^{\pm}(0)$, $E^{\pm}(z)$, and $E^{\pm}(L)$ become

$$\begin{pmatrix} E_l^+(z) \\ E_l^-(z) \end{pmatrix} = \begin{pmatrix} F_{11}(z)e^{-j\beta_0 z} & F_{12}(z)e^{-j\beta_0 z} \\ F_{21}(z)e^{j\beta_0 z} & F_{22}(z)e^{j\beta_0 z} \end{pmatrix} \begin{pmatrix} E^+(0) \\ E^-(0) \end{pmatrix} = \begin{pmatrix} a_{l11}(z) & a_{l12}(z) \\ a_{l21}(z) & a_{l22}(z) \end{pmatrix} \begin{pmatrix} E^+(0) \\ E^-(0) \end{pmatrix} \quad (12)$$

and

$$\begin{pmatrix} E^+(L) \\ E^-(L) \end{pmatrix} = \begin{pmatrix} F_{11}(L-z)e^{-j\beta_0(L-z)} & F_{12}(L-z)e^{-j\beta_g(L+z)} \\ F_{21}(L-z)e^{j\beta_0(L+z)} & F_{22}(L-z)e^{j\beta_g(L-z)} \end{pmatrix} \times \begin{pmatrix} E_r^+(z) \\ E_r^-(z) \end{pmatrix} = \begin{pmatrix} a_{r11}(L-z) & a_{r12}(L-z) \\ a_{r21}(L-z) & a_{r22}(L-z) \end{pmatrix} \begin{pmatrix} E_r^+(z) \\ E_r^-(z) \end{pmatrix}. \quad (13)$$

Here, L is the cavity length. Then, equivalent reflectivity $\rho_l(z)$, $\rho_r(z)$ and equivalent transmittance $t_r(z)$ at the coordinate z, which are schematically depicted in Fig. 1 are given as:

$$\rho_l(z) = \frac{E_l^+(z)}{E_l^-(z)} = \frac{r_l a_{l11}(z) + a_{l12}(z)}{r_l a_{l21}(z) + a_{l22}(z)} \quad (14)$$

$$\rho_r(z) = \frac{E_r^-(z)}{E_r^+(z)} = -\frac{r_r a_{r11}(L-z) - a_{r21}(L-z)}{r_r a_{r12}(L-z) - a_{r22}(L-z)} \quad (15)$$

$$t_r(z) = \frac{E_r^+(L)}{E_r^+(z)}$$

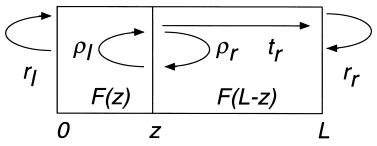

Fig. 1 Schematic picture showing equivalent reflectivities and transmittance, $\rho_l(z)$, $\rho_r(z)$, $t_r(z)$, and other parameters.

$$= \frac{a_{r11}(L-z)a_{r22}(L-z) - a_{r12}(L-z)a_{r21}(L-z)}{a_{r22}(L-z) - a_{r12}r_r} \quad (16)$$

in which r_l and r_r are the amplitude reflection coefficients of rear (left-hand-side) and front (right-hand-side) facets. Note that $E_{l,r}^{\pm}(z)$ are variables introduced for the sake of convenience. $E_l^-(z)$ and $E_l^+(z)$ mean light amplitudes incident into and reflected out of the cavity's left-hand-side portion (0 to z) at the "virtual" facet z (see Fig. 1) whereas $E_r^+(z)$ and $E_r^-(z)$ mean those incident into and reflected out of the right-hand-side portion (z to L) at z.

If spontaneous emission having unit amplitude occurred at the coordinate z, the electric field observed at the front facet due to that emission toward right-hand side should be expressed as

$$t_r + (\rho_r\rho_l)t_r + (\rho_r\rho_l)^2 t_r + \cdots = \frac{t_r}{1-\rho_l\rho_r} \quad (17)$$

and the electric field due to the spontaneous emission toward left-hand side should be

$$\rho_l t_r + (\rho_l\rho_r)\rho_l t_r + (\rho_l\rho_r)^2\rho_l t_r + \cdots = \frac{\rho_l t_r}{1-\rho_l\rho_r}. \quad (18)$$

Assuming that the spontaneous emission is occurring uniformly and randomly throughout the cavity, relative output intensity is calculated by integrating absolute of Eqs. (17) and (18) over $z = 0$ to L:

$$\int_0^L \frac{|t_r|^2(1+|\rho_l|^2)}{|1-\rho_l\rho_r|^2}(1-|r_r|^2)dz. \quad (19)$$

By repeating this calculation for different wavelengths, theoretical sub-threshold spectrum is obtained. Since the sum of the infinite geometric series is used in Eqs. (17) and (18), $|\rho_l\rho_r|$ should be less than unity. Therefore, this spectrum calculation is only applicable to "sub-threshold" condition.

2.2 Parameters

There are thirteen parameters involved in the model of sub-threshold spectrum. Some of them are able to be extracted, and others need to be known from the beginning. The parameters that can be extracted by our extraction method are:

- index coupling (IC) coefficient : κ_i
- gain coupling (GC) coefficient : κ_g

- parameters associated with net gain profile : g_1, g_2, and λ_p
- parameters associated with effective refractive index : n_{Bragg} and $\frac{dn}{d\lambda}$
- facet phases of the grating : θ_l and θ_r

On the other hand, the following parameters need to be fixed:

- cavity length : L
- grating period : Λ
- facet intensity reflectivities : $R_l(=|r_l|^2)$ and $R_r(=|r_r|^2)$

Here, the net gain profile is assumed to have a parabolic shape, namely,

$$g(E) = g_1 - g_2\left(E - \frac{hc}{q\lambda_p}\right)^2 \tag{20}$$

and the effective refractive index is assumed to have linear wavelength dispersion, namely,

$$n_{eff}(\lambda) = n_{Bragg} + \frac{dn}{d\lambda}(\lambda - \lambda_{Bragg}). \tag{21}$$

3. Parameter Extraction Procedure

3.1 Least-Square Algorithm

Numerical fitting is done on the basis of the least-square algorithm. Let $\boldsymbol{a}$ indicate parameter vector, like $\boldsymbol{a} = (\kappa_i, \kappa_g, g_1, \ldots)$, $y_m(\lambda_i)$ indicate measured spectrum data at λ_i, and $y_c(\lambda_i; \boldsymbol{a})$ indicate calculated spectrum using one parameter set $\boldsymbol{a}$. N is the number of sampling points. Then, the least-square algorithm find the parameter set $\boldsymbol{a}_{fit}$ which minimizes σ^2, that is,

$$\sigma^2 \equiv \frac{1}{N}\sum_{i=1}^{N}\{y_m(\lambda_i) - y_c(\lambda_i; \boldsymbol{a})\}^2. \tag{22}$$

To perform the algorithm, we used the routine called "NL2SOL", one of general nonlinear least-square programs [9]. This routine takes care of the minimization of σ^2. In doing that, it generally requires two subroutines, one for calculating σ, and the other for $\partial\sigma/\partial a_k$. Therefore we prepared subroutine that calculates the sub-threshold spectrum $y_c(\lambda_i; \boldsymbol{a})$, and another that calculates its deviation $\partial y_c(\lambda_i; \boldsymbol{a})/\partial a_k$.

3.2 Initial Parameters Determination

When doing numerical fitting, initial parameters, with which the above mentioned least-square algorithm is started, are very important. Those values need to be close enough to the final value, in order for the fitting values to converge. Success or failure in parameter extraction really depends on the determination of initial parameters. Our initial values are derived by the following procedure:

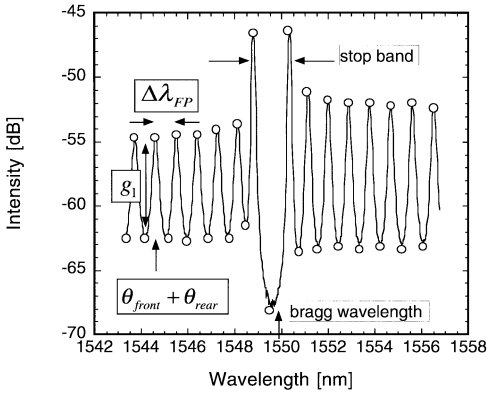

Fig. 2 Obtaining initial parameter sets.

1. Read peaks and valleys from the measured spectrum, and estimate average Fabry-Perot (FP) mode spacing $\Delta\lambda_{FP}$ (see Fig. 2).
2. Read stop-band from the widest mode spacing, and regard the center of the stop-band as the Bragg wavelength λ_{Bragg}.
3. If cavity length L and grating pitch Λ are given, the effective refractive index at the Bragg wavelength n_{Bragg} and its wavelength dispersion $dn/d\lambda$ are calculated as:

$$n_{Bragg} = \frac{\lambda_{Bragg}}{2\Lambda} \tag{23}$$

$$\frac{dn}{d\lambda} = \frac{n_{Bragg}}{\lambda_{Bragg}} - \frac{\lambda_{Bragg}}{2L\Delta\lambda_{FP}}. \tag{24}$$

   The effective refractive index, n_{eff}, is $n_{Bragg} + \frac{dn}{d\lambda}(\lambda - \lambda_{Bragg})$.
4. When both facets are as cleaved, facet reflectivities, R_{front} and R_{rear}, are calculated by the following equation and fixed throughout the fitting procedure.

$$R_{front} = R_{rear} = \left(\frac{n_{Bragg} - 1}{n_{Bragg} + 1}\right)^2 \tag{25}$$

5. From the shortest wavelength among observed FP peaks, which is influenced by DFB mode least, sum of the both facet phases is calculated as

$$\theta_{rear} + \theta_{front} = \frac{\mathrm{mod}(\beta \cdot 2L, 2\pi)\lambda_{short}}{2n_{eff}\Lambda} \tag{26}$$

   where θ_{front} is assumed to be zero as a starting value.
6. From relation between stop-band width and index coupling coefficient with no facet reflectivity calculated beforehand as shown in Fig. 3, the index coupling coefficient can be expressed as

$$\kappa_i = 0.68025\delta - 2.6206/L. \tag{27}$$

   The starting value for the index coupling coefficient is calculated using this formula.

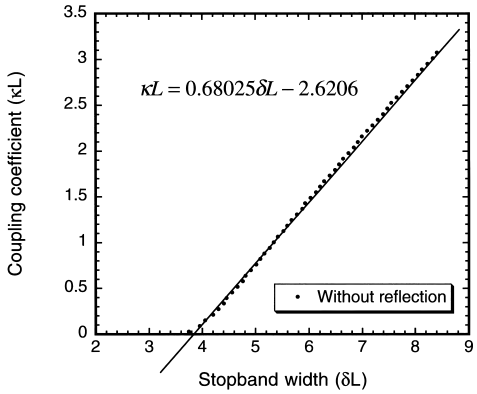

Fig. 3 Relation between stop-band δL and index coupling coefficient $\kappa_i L$, when there is no facet reflection. The relation is approximated by a linear function shown as an inset.

7. From the peak and valley powers, P^+ and P^-, of the FP mode with the shortest wavelength, net gain can be calculated as [13]

$$g_1 = \frac{1}{L}\left\{\ln\frac{\sqrt{10^{P^+/10}}-\sqrt{10^{P^-/10}}}{\sqrt{10^{P^+/10}}+\sqrt{10^{P^-/10}}} + \ln\frac{1}{\sqrt{R_{front}}\sqrt{R_{rear}}}\right\} \quad (28)$$

   where the powers are in dB, and g_2 in Eq. (20) is zero as an initial value.
8. Gain peak wavelength λ_p is set to the Bragg wavelength at the beginning.
9. The initial value of the gain coupling coefficient, κ_g, is set to zero.

3.3 Results of Parameter Extraction

One good way of checking the reliability of the parameter fitting is to extract parameters from the front facet spectrum and from the rear facet one independently, and compare the corresponding values. Spectra from front and rear facets have different shapes because of asymmetry in the facet phase.

The sample measured here was a $1.55\,\mu$m InGaAsP/InP compressively-strained MQW gain-coupled DFB laser of absorptive grating type, with cleaved facets and a $550\,\mu$m long cavity. Figures 4(a) and (b) show measured spectra as well as calculated ones (initial and fitted) from the front and rear facets of the same device. The initial and final (extracted) parameters are listed in Table 1. Although the fittings were done independently and the shapes of the spectra done independently and the shapes of the spectra were different, the extracted parameters for the front and rear facet spectra agreed well. Reliability of this method is confirmed thereby.

In doing the calculation, all the parameters were assumed to be uniform along the cavity. However, if

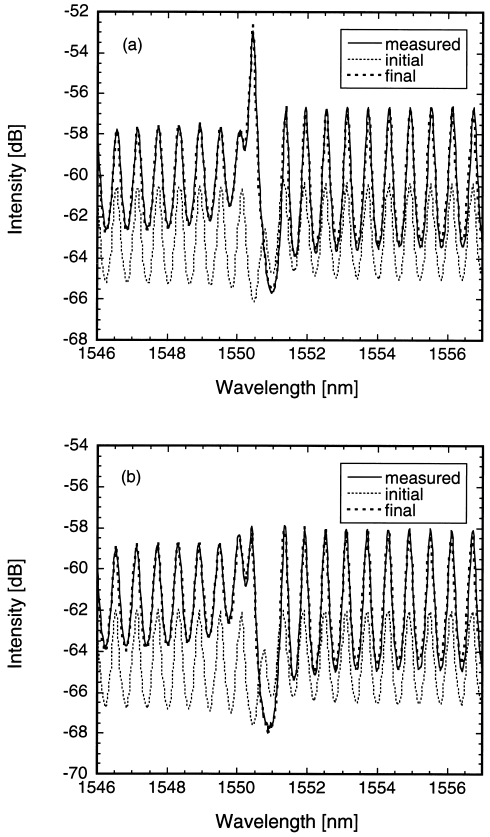

Fig. 4 Spectra from front (a) and rear (b) facets in a $1.55\,\mu$m InGaAsP/InP GC DFB laser of absorptive grating type (I=24 mA).

Table 1 Starting and fitted values of parameters in a GC-DFB laser (I=24 mA).

Parameter [unit]	front		rear	
	init.	fitted	init.	fitted
g_1 [cm^{-1}]	−1.1	3.3	−1.1	3.0
g_2 [μm^{-1}eV^2]	0	6	0	13
λ_p [nm]	1551	1557	1551	1553
n_{Bragg}	3.27	3.27	3.27	3.27
$dn/d\lambda$ [μm^{-1}]	−0.249	−0.250	−0.249	−0.249
κ_i [cm^{-1}]	10.5	27.9	9.4	28.1
κ_g [cm^{-1}]	0	−4.6	0	−4.2
θ_{rear} [degree]	106	−177	100	−176
θ_{front} [degree]	0	149	0	144

$$g = g_1 - g_2\left(E - \frac{hc}{q\lambda_p}\right)^2, \quad n = n_{Bragg} + \frac{dn}{d\lambda}\left(\lambda - \lambda_{Bragg}\right)$$

spatial hole burning occured, this assumption would not hold. In order to check it, field intensity profile along the cavity is calculated using extracted parameters listed in Table 1. In Fig. 5, the field intensity profiles of the two modes on both sides of the stop band are plotted, where one on the shorter wavelength side is indicated by thin solid lines, and the other on the longer wavelength side by dotted lines. Lines with right and left arrows indicate the intensity of forward and

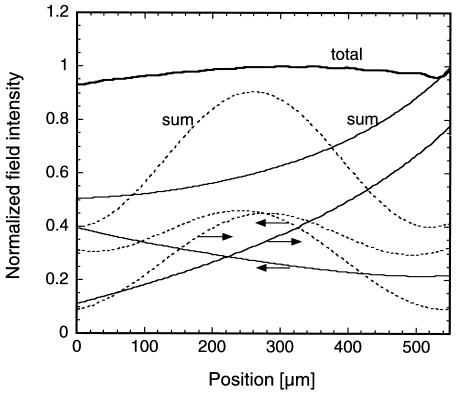

Fig. 5 Intensity profiles along the cavity for the GC-DFB laser in Fig. 4. Thin solid and dotted lines correspond to those for the modes on the shorter wavelength side and longer wavelength side of the stop band, respectively. The thick solid line is for the overall intensity profile including those of many FP modes.

backward propagating wave, and lines labeled "sum" are the sum of the forward and backward propagation waves. The line labeled "total" is the overall intensity including other FP modes. Each line is normalized. Only the "total" line has a different normalization factor and therefore should not be compared with other lines in terms of absolute value.

From the "total" profile, one may notice that there is no significant spatial hole burning occuring. The reason is that, below threshold, there are many FP mode coexisting with DFB modes whose intensity distribution is almost uniform over the cavity length. One more thing to be noted in Fig. 5 is the intensity difference between the shorter-wavelength-side mode and the longer-wavelength-side one; the difference is large at the front facet whereas it is small at the rear facet. This situation resulted in the shapes of the spectrum in Figs. 4(a) and (b).

4. Error Assessment

Now that many parameters are derived only from the sub-threshold spectrum, we then estimate how accurate these extracted parameters are.

First, we define σ_{min} and χ as:

$$\sigma_{min}^2 \equiv \frac{1}{N}\sum_i^N \{y_m(\lambda_i) - y_c(\lambda_i; \boldsymbol{a}_{fit(0)})\}^2 \qquad (29)$$

$$\chi^2 \equiv \sum_i^N \left\{ \frac{y_m(\lambda_i) - y_c(\lambda_i; \boldsymbol{a})}{\sigma_{min}} \right\}^2 . \qquad (30)$$

By numerical fitting to the measured data $D_{(0)}$, $\boldsymbol{a}_{fit(0)}$ is determined by minimizing χ^2 through $\boldsymbol{a}$ adjustment. Here, (0) denotes measurement and fitting without noise disturbance. Then χ^2_{min} is obtained as

$$\chi^2_{min} \equiv \sum_i^N \left\{ \frac{y_m(\lambda_i) - y_c(\lambda_i; \boldsymbol{a}_{fit(0)})}{\sigma_{min}} \right\}^2 . \qquad (31)$$

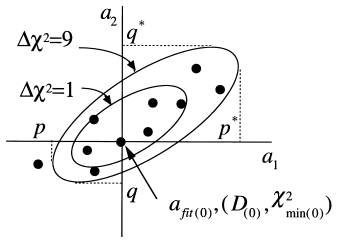

Fig. 6 Schematic showing how error bars of each fitted paramters are derived.

If random noise is added while measurement, the data set D becomes different and the extracted parameter set $\boldsymbol{a}_{fit}$ is also changed. That is, $\boldsymbol{a}_{fit}$ is distributed around $\boldsymbol{a}_{fit(0)}$. When the values of the parameter set are changed to $\boldsymbol{a}_{fit(0)} + \Delta\boldsymbol{a}$, the value of χ^2 is also changed to $\chi^2_{min} + \Delta\chi^2$.

According to the statistics, when noise of these measured data has normal distribution, 99.73% (3σ of normal distribution) of $\boldsymbol{a}_{fit}$ is contained within the region of $\Delta\chi^2 = 9$. In our case, the measured spectra do not necessarily have normal distribution. Nevertheless, this model is used in order to assess the error of fitting quantitatively. For example, error ranges of two parameters, a_1 and a_2, in Fig. 6 are $p \le a_1 \le p^*$ and $q \le a_2 \le q^*$. Error bars in the following figures are thus calculated.

5. Current Dependence of Coupling Coefficients

Next, we investigated injection current dependence of these device parameters. Figures 7 (a), (b), 8 (a), and (b) are the results corresponding to gain- and index-coupling coefficients, κ_g and κ_i, and front- and rear-facet phases, θ_{front} and θ_{rear}, respectivily. Sub-threshold spectra were measured from both front and rear facets, and parameter extraction was carried out on the spectra independently. Resulting fitted parameters for the front and rear facet spectra are shown in the same graphs. Minus sign of κ_g indicates "anti-phase" complex coupling.

In Figs. 8(a) and (b), one can see that the facet phases of the grating extracted from front and rear facet specta agree very well and that they don't change with current. These results are quite reasonable and let us confirm the reliability of our parameter extraction. In Figs. 7(a) and (b), we notice that the magnitudes of κ_g and κ_i become small as injection current increases. The change of κ_g is considered to be due to saturated absorption of the grating. As the number of photons is increased, absorption coefficient of the grating becomes saturated, thus making $|\kappa_g|$ small. On the other hand, the change of κ_i is because of the band-filling effect: as the number of photons absorbed in the grating increases, refractive index of the grating becomes small due to carrier generation. Since the refractive index of

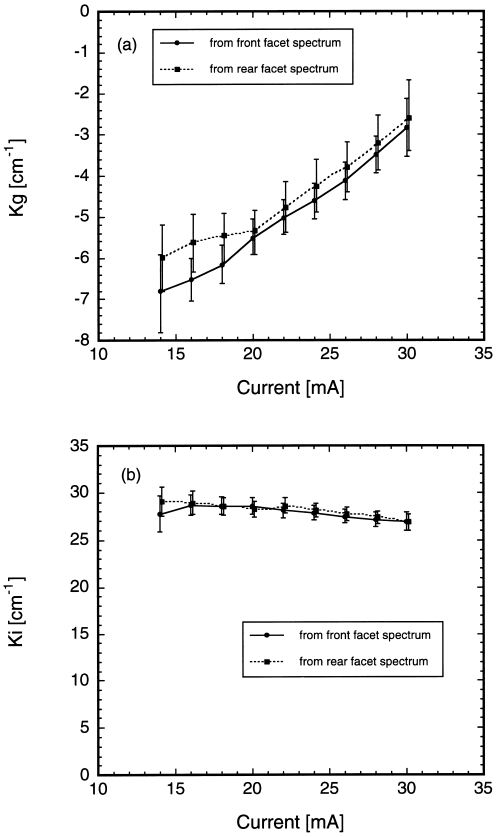

Fig. 7 Injection current dependences of gain coupling coefficient, κ_g, (a), and index coupling coefficient, κ_i, (b), in the 1.55 μm InGaAsP/InP GC DFB laser of absorptive grating type.

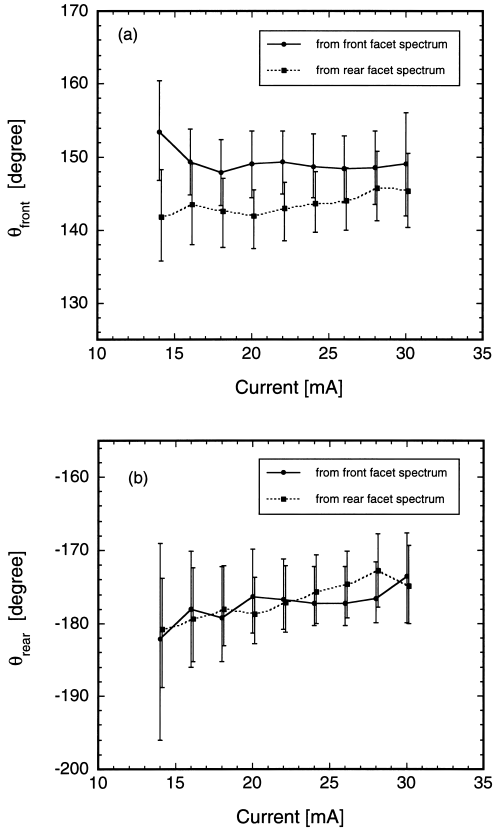

Fig. 8 Injection current dependences of front facet phase, θ_{front}, (a), and rear facet phase, θ_{rear}, (b), in the 1.55 μm InGaAsP/InP GC DFB laser of absorptive grating type.

the absorptive grating is higher originally, this leads to κ_i reduction.

The same measurement was done on an index-coupled DFB laser. The sample measured here was a 1.55 μm InGaAsP/InP compressively-strained MQW index-coupled (IC) DFB laser without absorptive grating, with cleaved facets and a 440 μm long cavity.

Like in Fig. 4, the sub-threshold spectra for front and rear facets look different in a single device due to asymmetry in facet grating phases in Figs. 9(a) and (b). Nevertheless, the extracted parameters in Figs. 10 and 11 are almost the same for both cases. Moreover, the facet phase values extracted for different currents in Figs. 11(a) and (b) do not differ very much with each other. This again shows the reliability of our program.

It should be noted that the extracted index coupling coefficient, κ_i, in Fig. 10(a) does not depend on injection current level unlike before. This is reasonable since the cause of changing κ_i in the previous GC-DFB laser's case was photon absorption in the absorptive grating, which is not present in this IC-DFB laser. In addition, the extracted value of κ_g in Fig. 10(b) is almost zero, which is another evidence that our parameter extraction method is able to differentiate IC and GC, and to give correct κ_g values.

6. Conclusions

We have developed a reliable, automatic, and nondestructive parameter extraction program for both gain- and index-coupled DFB lasers with finite facet reflectivities, and named it as "LAPAREX" (LAser PArameter EXtraction). This program allows extraction and determination of such parameters as gain- and index-coupling coefficients, and spatial phases of the grating at the front and rear facets, from measured sub-threshold spectra. By making use of this program, injection current dependence of coupling coefficients in a gain-coupled DFB laser of absorptive grating type was detected and measured for the first time. Through the measurement of gain coupling coefficients, which has not been possible so far, structural optimization of gain-coupled DFB lasers would become feasible. Therefore, this program is a key tool for achieving better performance in DFB lasers. The program (for PCs and Macintoshes) can be downloaded and tested from http://www.ee.t.u-tokyo.ac.jp/ nakano/lab/welcome.html.

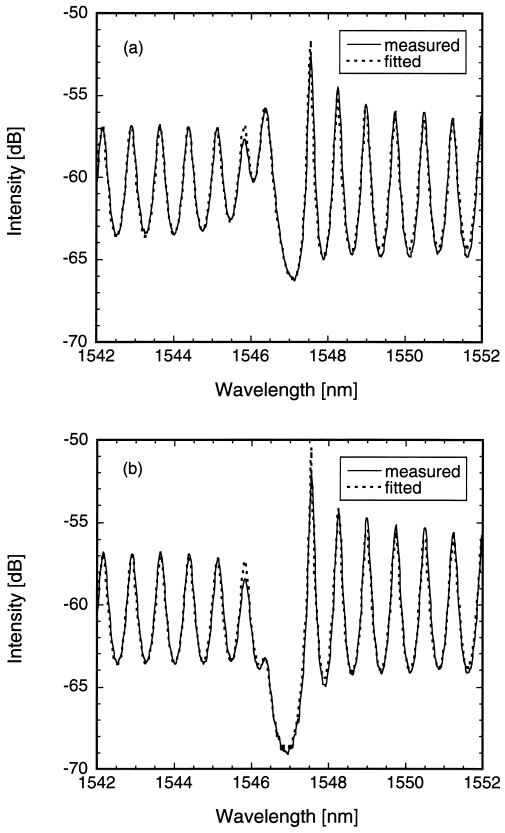

Fig. 9 Spectra from front (a) and rear (b) facets in a 1.55 μm InGaAsP/InP IC DFB laser (I=3 mA).

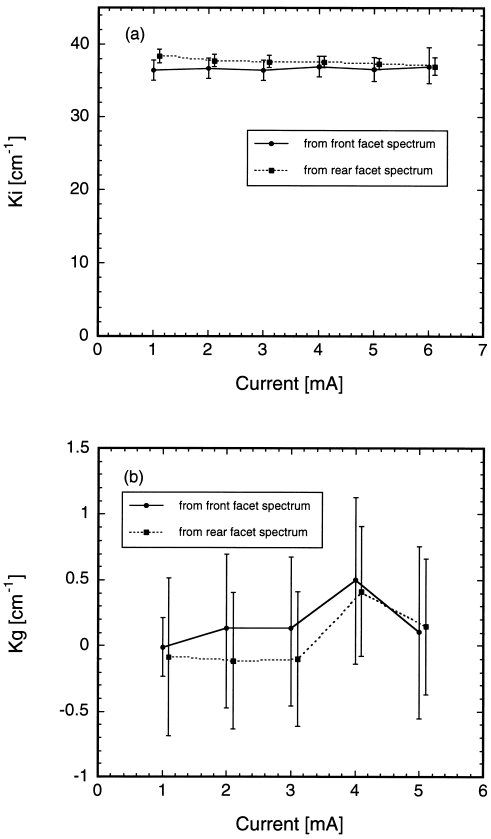

Fig. 10 Injection current dependences of index coupling coefficient, κ_i, (a), and gain coupling coefficient, κ_g, (b), in the 1.55 μm InGaAsP/InP IC DFB laser.

Acknowledgement

The authors would like to thank Prof. Roel Baets and Dr. Geert Morthier of the University of Gent, Belgium, and Dr. Kenji Sato of NEC Kansai Electronics Laboratories as this research was initiated in collaboration with them. The authors are also grateful to Prof. Kunio Tada of Yokohama National University for encouragement.

References

[1] S.R. Chinn, "Effects of mirror reflectivity in a distributed-feedback laser," IEEE J. Quantum Electron., vol.QE-9, no.6, pp.574–580, June 1973.

[2] L.J.P. Ketelsen, I. Hoshino, and D.A. Ackerman, "Experimental and theoretical evaluation of the CW suppression of TE side modes in conventional 1.55 μm InP-InGaAsP distributed feedback lasers," IEEE J. Quantum Electron., vol.27, no.4, pp.965–975, April 1991.

[3] D.M. Adams, D.T. Cassidy, and D.M. Bruce, "Scanning photoluminescence technique to determine the phase of the grating at the facets of gain-coupled DFB's," IEEE J. Quantum Electron., vol.32, no.7, pp.1237–1242, July 1996.

[4] G. Morthier, K. Sato, R. Baets, T.K. Sudoh, Y. Nakano, and K. Tada, "Parameter extraction from subthreshold spectra in cleaved gain- and index-coupled DFB LDs," Tech. Digest, Conf. on Optical Fiber Communication (OFC'95), pp.309–310, March 1995.

[5] T. Nakura, K. Sato, M. Funabashi, G. Morthier, R. Baets, Y. Nakano, and K. Tada, "First observation of changing coupling coefficients in a gain-coupled DFB laser with absorptive grating by automatic parameter extraction from subthreshold spectra," Tech. Digest, Conf. of Lasers and Electro-Optics (CLEO'97), pp.135–136, May 1995.

[6] H. Kogelnik and C.V. Shank, "Coupled-wave theory of distributed feedback lasers," J. Appl. Phys., vol.43, no.5, pp.2327–2335, May 1972.

[7] T. Makino and J. Glinski, "Transfer matrix analysis of the amplified spontaneous emission of DFB semiconductor laser amplifiers," IEEE J. Quantum Electron., vol.24, no.8, pp.1507–1518, Aug. 1988.

[8] P. Vankwikelberge, G. Morthier, and R. Beats, "CLADISS —A longitudinal multimode model for the analysis of the static, dynamic, and stochastic behavior of diode lasers with distributed feedback," IEEE J. Quantum Electron., vol.26, no.10, pp.1728–1741, Oct. 1990.

[9] J.E. Dennis, Jr., D.M. Gay, and R.E. Welsch, "An adaptive nonlinear least-squares algorithm," ACM Trans. on Mathematical Software, vol.7, no.3, pp.348–368, Sept. 1981.

[10] A. Yariv and M. Nakamura, "Periodic structures for integrated optics," IEEE J. Quantum Electron., vol.QE-13, no.4, pp.233–253, April 1977.

[11] Y. Nakano, Y. Luo, and K. Tada, "Facet reflection independent, single logitudinal mode oscillation in a GaAlAs/GaAs distributed feedback laser equipped with a gain-coupling mechanism," Appl. Phys. Lett., vol.55, no.16, pp.1606–1608, Oct. 1989.

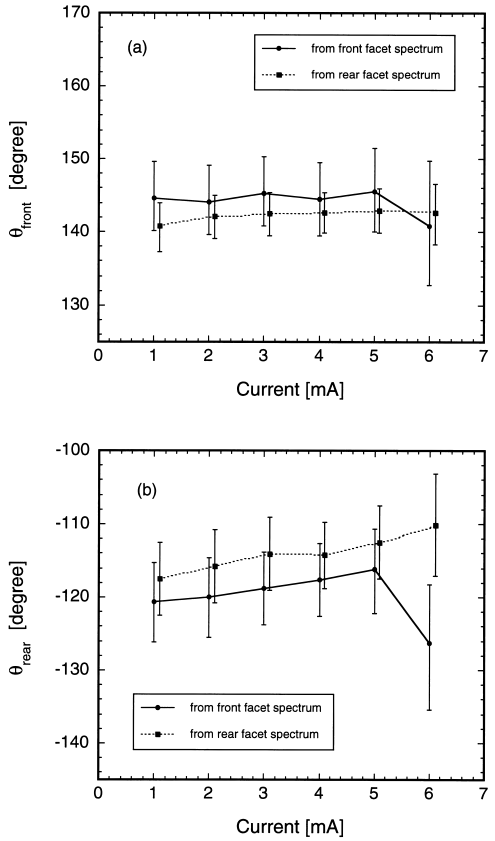

Fig. 11 Injection current dependences of front facet phase, θ_{front}, (a), and rear facet phase, θ_{rear}, (b) in the 1.55 μm InGaAsP/InP IC DFB laser.

[12] H. Soda and H. Imai, "Analysis of the spectrum behavior below the threshold in DFB lasers," IEEE J. Quantumn Electron., vol.QE-22, no.5, pp.637–641, May 1986.
[13] B.W. Hakki and T.L. Paoli, "Gain spectra in GaAs double-heterostructure injection lasers," J. Appl. Phys., vol.46, no.3, pp.1299–1306, March 1975.

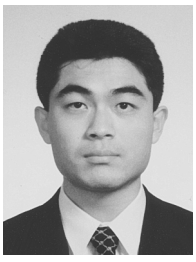

Toru Nakura was born in Fukuoka, Japan in 1972. He received the B.S. and M.S. degrees in electronic engineering from Uiniversity of Tokyo, Japan, in 1995 and 1997, respectively. From 1995 to 1997, he was engaged in device modeling of distributed feedback lasers. From 1997, he worked for System LSI Development Center in Mitsubishi Electric Corporation for two years where he designed high-speed communication circuits. He is currently working for Avant! Corporation and has been developing a EDA tool for VLSI circuit design.

Yoshiaki Nakano received the B.E., M.S., and Ph.D. degrees in electronic engineering, all from the University of Tokyo, Japan, in 1982, 1984, and 1987, respectively. In 1984, he spent a year at the University of California, Berkeley, as an exchange student. In 1987, he joined the School of Engineering, the University of Tokyo, and is currently an Associate Professor with the Department of Electronic Engineering. His research interests have been physics and fabrication technologies of semiconductor distributed feedback lasers, optical modulators/switches, and photonic integrated circuits. In 1992, he was a visiting Associate Professor at the University of California, Santa Barbara. Dr. Nakano is a member of IEEE, Optical Society of America, the Japan Society of Applied Physics (JSAP), and the Japan Institute of Electronics Packaging (JIEP). He is the recipient of the 1987 Shinohara Memorial Prize from the IEICE, the 1991 Optics Paper Award from the JSAP, and the 1997 Marubun Science Prize.